Journal of Alloys and Compounds 595 (2014) 60–66

Contents lists available at ScienceDirect

Journal of Alloys and Compounds

journal homepage: www.elsevier.com/locate/jalcom

Effect of particle size and oxygen content of Si on processing, microstructure and thermal conductivity of sintered reaction bonded Si_3N_4

Brahma Raju Golla [a,b], Jae Woong Ko [a,*], Jin-Myung Kim [a], Hai-Doo Kim [a]

[a] Engineering Ceramics Research Group, Korea Institute of Materials Science, Changwon, Gyeongnam 642-831, Republic of Korea
[b] Metallurgical and Materials Engineering Department, National Institute of Technology Warangal, Andhra Pradesh 506004, India

ARTICLE INFO

Article history:
Received 12 November 2013
Received in revised form 16 January 2014
Accepted 17 January 2014
Available online 27 January 2014

Keywords:
Reaction-bonded Si_3N_4
Gas pressure sintering
Densification
Microstructure
Thermal conductivity

ABSTRACT

In the ceramic processing, use of the fine powders is more desirable in order to enhance densification and eventually the properties of ceramics. However, during the particle size reduction (using ball milling), the powders are also prone to surface oxidation. In this perspective, the present contribution systematically investigates the influence of Si particle size and its oxygen content on nitridation, densification, microstructure and thermal conductivity of sintered reaction bonded Si_3N_4 (SRBSN) mixed with 3.5% Y_2O_3–1.5% MgO (sintering additive). Despite it's relatively low density, the SRBSN sample with Si as received powders exhibited high thermal conductivity when compared to SRBSN with planetary ball milled samples. A maximum thermal conductivity of ~90 W/m K was measured for the SRBSN sample (using high purity Si as received powders) after gas pressure sintering at 1950 °C for shorter sintering time of 3 h. It is a promising result as far as the industrial applications are concerned. Normally in the literature very high sintering temperatures and extensive sintering times were reportedly used for obtaining high thermal conductivity of Si_3N_4 ceramics. In the present work, the improvement in thermal conductivity of the SRBSN with Si as received powders can be attributed to its coarse grain microstructure, large elongated β-Si_3N_4 grains, relatively small amount of grain boundary phase (mainly because of low amount of oxygen in starting raw Si powders when compared to Si planetary ball milled powders) and large phonon scattering distance. As far as the thermal transport properties are concerned, the present research reveals that the use of Si powders with moderate particle size and low amount of oxygen is beneficial to improve the thermal conductivity of SRBSN.

1. Introduction

Silicon nitride (Si_3N_4) ceramics have been widely studied for various structural applications (both at room and high temperatures) as they exhibit excellent mechanical properties, good refractoriness, very high resistance to thermal shock and chemical attack, excellent creep resistance, good tribological and wear properties [1–4]. In the last two decades, considerable research efforts have been directed in developing Si_3N_4 with high thermal conductivity and good mechanical properties in view of its potentiality for power electronic device applications [1,5,6]. Historically AlN has been used as circuit substrates of power devices as it exhibits high thermal conductivity of more than 200 W/m K [6,7]. However, its low mechanical properties (bending strength: 300–400 MPa and fracture toughness: 3–4 MPa $m^{1/2}$) results in low reliability. Hence in the recent past, Si_3N_4 has been tried as an alternative substrate material for electronic devices [5,6,8,9].

It is well known that Si_3N_4 can be processed either sintering directly Si_3N_4 starting powders (SSN) or via reaction bonded Si_3N_4 (RBSN) [3]. In the RBSN processing route, Si powder compact is heat treated in nitrogen atmosphere to transform it into Si_3N_4 and post sintering of the nitride sample may be required for further enhancement of densification [10]. Nitridation is typically carried out in a nitrogen or nitrogen-containing atmosphere between the temperatures of 1200–1450 °C. In order to control the rate of development and the exothermicity of the reaction, and the thermal properties and molecular diffusivity of the gas; hydrogen, helium, or argon can be added to the nitrogen gas. The RBSN materials have been studied extensively since the 1970s [10–29]. However, they were not considered as good structurally as sintered Si_3N_4 ceramics since RBSN materials did not have good mechanical

* Corresponding author. Tel.: +82 9549654563.
E-mail address: kjw1572@kims.re.kr (J.W. Ko).

http://dx.doi.org/10.1016/j.jallcom.2014.01.131
0925-8388/

properties as they contain 15–20 vol.% of porosity. In order to improve the mechanical properties of RBSN ceramics, sintering is an essential step after the nitridation. The sintered reaction bonded Si_3N_4 (SRBSN) has several advantages when compared to the conventional sintering of Si_3N_4-powder compacts. The low cost of SRBSN is due to low raw material cost and low costs of machining because of the lower sintering shrinkage and minimum distortions during post-sintering, the ability to produce complex shaped components with near-net-shape and with good mechanical properties [10–12,22,23].

Sintering additives such as rare earth oxides, SiO_2, Al_2O_3, ZrO_2, MgO and $MgSiN_2$ have been used to enhance densification and mechanical, thermal, oxidation properties of Si_3N_4 ceramics [3,4,24–29]. However, the use of SiO_2 and Al_2O_3 are not suitable for improving thermal conductivity of Si_3N_4 as they dissolve in β-Si_3N_4 lattice and thereby lower the thermal conductivity [30,31]. On the other hand, use of rare earth oxides (Y_2O_3, Yb_2O_3 etc.) in combination with MgO or $MgSiN_2$ has been widely studied in order to improve thermal conductivity of Si_3N_4 [32–35]. As far as the role of sintering additive is concerned, it promotes densification and enhances thermal conductivity by removing lattice oxygen. A careful review of literature reveals that the sintered Si_3N_4 (SSN) ceramics have relatively low thermal conductivity when compared to SRBSN ceramics [6,29]. It is mainly because of high amount of oxygen impurity presence in the starting Si_3N_4 powders. Nevertheless, it was possible to improve thermal conductivity of Si_3N_4 (more than 140 W/m K) using optimal amount of sintering additive and use of extreme sintering conditions along with annealing treatment [5,6,27–29,34].

Although Si_3N_4 with very high thermal conductivity is essentially required, in view of commercial applications of Si_3N_4, use of such extreme processing conditions is not desirable as it adds up to the processing cost. Hence in this work, we explored whether thermal conductivity can be improved via SRBSN route with controlling particle size of Si (in combination with Y_2O_3–MgO sintering additive) by employing suitable sintering conditions and reducing the sintering time duration. It has to be noted here that in the present work, the Y_2O_3–MgO is selected as a sintering additive as it was reported to be very effective in improving densification, thermal conductivity and mechanical properties of Si_3N_4 ceramics [5,29–32]. In the present study, high purity Si powders with different particle sizes of 4.60 μm (Si as received) and 0.43 μm (Si particle size was reduced by planetary ball milling) were used. The effect of Si particle size and its oxygen content on nitridation, densification, microstructure and thermal conductivity of sintered reaction bonded Si_3N_4 (SRBSN) mixed with 3.5 wt.% Y_2O_3–1.5 wt.% MgO was systematically studied. The thermal conductivity of SRBSN samples is correlated with the microstructure and the phonon mean free path in view of understanding the heat conduction mechanisms.

2. Experimental details

Commercially available high purity Si powder (99.9999%), MgO (Sigma–Aldrich, 99.99%) and Y_2O_3 (Grade C, H.C. Starck GmbH and Co., Goslar, Germany) were used as starting materials. The amount of sintering additives and the mass ratios between Y_2O_3:MgO were fixed to 5 wt.% and 3.5:1.5 by weight, respectively. The starting Si powder had an average particle size (D_{50}) of 4.60 μm with an impurity content of 0.91 wt.% O_2. The particle size of the powders were measured using laser diffraction particle size analyzer (LS 13 320, Beckman Coulter). In order to study the size effect of Si, the Si powders were crushed with planetary mill at 300 rpm for 10 h using ethanol and Si_3N_4 balls as milling media. After milling, the Si powder had D_{50} of 0.43 μm and O_2 of 2.27 wt.%. From this it can be realized that the oxygen content of Si powders is significantly increased along with particle size reduction during milling. The increase in oxygen content can be attributed to the oxidation of the newly formed Si surfaces that are formed by fracture of particles during milling. This increased amount of oxygen is expected to exist mainly as surface oxide layer (SiO_2) on the powders. The SEM micrographs and particle size distribution of the Si as received and Si planetary ball milled powders are shown in Fig. 1. The Si as received powders are characterized by faceted morphology, whereas the Si planetary ball milled powders are very fine and agglomerated in the form. In both the cases, the Si powders are narrowly distributed (Fig. 1b and d). The sintering additives were crushed with planetary mill at 300 rpm for 10 h using ethanol and Si_3N_4 as milling media. Finally, the powders in appropriate amount were mixed by wet ball-milling for 3 h in a polyethylene bottle (for material compositions with Si planetary ball milled powders)/nylon jar (for material compositions with Si as received powders), using Si_3N_4 balls and ethanol as media. After the vacuum drying and sieving, approximately 0.7 g of the mixed powder was pressed into circular disc (~15 mm in diameter and 2.7 mm of thickness) using a stainless steel die, followed by cold isostatic pressing at 200 MPa. According to the geometry method, the compositions prepared using Si as received and Si planetary ball milled powders have green densities of 1.35 and 1.42 g/cm^3, respectively, corresponding to 56.01% and 59.04% theoretical densities (ρ_{th}), respectively.

The Si compacts were nitrided in an alumina tube furnace with a flowing mixed gas (N_2:H_2 = 95:5) of flow rate 0.15 L/min at final nitridation temperature of 1450 °C for 2.5 h. In fact, the nitridation process of the compacts is carried out over a range of temperature from room temperature (RT) to 1450 °C (i.e. RT, 600 °C, 1200 °C, 1300 °C,1350 °C, 1450 °C) with different heating rate/cooling rate and soaking time schedule for the total time duration of 36 h for the nitridation process. The nitride samples were placed in a BN-coated graphite crucible which was completely filled with 50BN–50Si_3N_4 as a packing powder and the sintering was carried out in a graphite resistance furnace (GPS, FPW 100/150-2200-100-LA, Elatec Inc., Andover, MA, USA). The post sintering of the samples was performed at 1850, 1900 and 1950 °C for 3 h under N_2 gas pressure of 2–5 MPa. The gas pressure was set at 2 MPa at room temperature and was increased to 5 MPa at the sintering temperature. The heating rate was set at 10 °C/min and the samples were cooled by turning off the furnace power.

The microstructure of nitrided and gas pressure sintered samples were observed using scanning electron microscopy (SEM) (JSM-5800, JEOL, Tokyo, Japan) and their phase identification was performed on the cross section of the samples using X-ray powder diffraction (XRD) (D/MAX 2200, Rigaku, Tokyo, Japan) with Cu Kα radiation of 36 kV and 26 mA. Additionally the quantitative analysis of α- and β-Si_3N_4 phase was also calculated according to the method reported by Delvin and Amin [36].

Thermal diffusivity of the Si_3N_4 samples (15 mm diameter and 1 mm thickness) was measured at room temperature using the laser-flash method (Netzsch LFA 457, Selb, Germany). Prior to thermal diffusivity measurements, the samples were grinded and polished on both sides, the surface of the samples was coated with carbon by spraying colloidal graphite to enhance the absorption of the flash energy. In this procedure, the front face of the disk sample is subjected to a short duration laser pulse and the thermal history of the opposite face is assessed. Each data point represents the mean of five individual measurements, with variation being <±0.1%. The thermal diffusivity (a), was calculated from the following expression,

$$a = 0.1338\frac{d^2}{t_{1/2}} \quad (1)$$

where d is the thickness of the specimen and $t_{1/2}$ is the half rise time to initiate the pulse in the test piece. The thermal conductivity (λ) of the samples was calculated based on the measured density (ρ), thermal diffusivity (a) and the specific heat values (C_p) according to the following equation:

$$\lambda = \rho a C_p \quad (2)$$

The specific heat values of the samples (gas pressure sintered at 1950 °C, for 3 h) are also measured using the laser-flash method (Netzsch LFA 457, Selb, Germany). A constant value of specific heat, 0.68 J/g K was used to calculate thermal conductivity for all the samples.

3. Results and discussion

3.1. Nitridation of Si compacts

The nitridation results of the RBSN samples are presented in Table 1. It is interesting to observe that both the samples are exhibiting different characteristics in terms of nitridation (%), β/(α + β) phase ratio, densification and linear shrinkage after the nitridation at 1450 °C, for 2.5 h. In particular, the RBSN sample with Si planetary ball milled powders shows high amount of β Si_3N_4 phase (63.2%), high relative density (71.1% ρ_{th}) and relatively more linear shrinkage (2.7%) and less nitridation rate (91.2%) when compared to the RBSN with Si as received sample. This indicates that the starting powder particle characteristics of the samples strongly influence the nitridation characteristics. As mentioned in the previous section, both the Si powders have significant differences with respect to particle size and oxygen content. The high density and

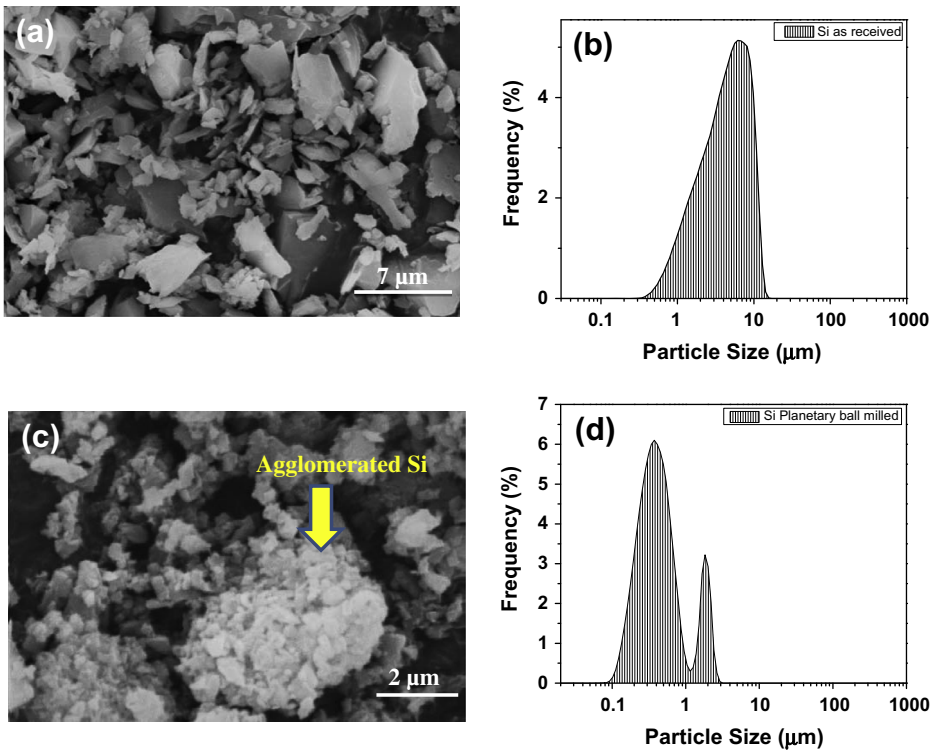

Fig. 1. SEM micrographs and particle size distributions of Si as-received and Si planetary ball milled powders. (a and b), Si as received powders; (c and d), Si planetary ball milled powders. The planetary ball milling of Si powders was carried out at 300 rpm for 10 h using ethanol and Si_3N_4 balls as milling media.

Table 1
Nitridation results of the Si compacts at 1450 °C, 2.5 h. (*Si as received represents (Si–3.5 wt.% Y_2O_3–1.5 wt.% MgO), where Si as received powders are used ; *Si planetary ball milled represents (Si–3.5 wt.% Y_2O_3–1.5 wt.% MgO) where Si powders are planetary ball milled).

Samples	Nitridation (%)	β/(α + β) (%)	Bulk density (g/cm^3)	Relative density (% ρ_{th})	Linear shrinkage (%)	XRD-phase assemblage
*Si as received	94.25	54.0	2.12	65.74	0.35	α Si_3N_4, β Si_3N_4, $Y_5Si_3O_{12}N$, $YSiO_2N$
*Si planetary ball milled	91.22	63.2	2.30	71.08	2.69	α Si_3N_4, β Si_3N_4, $Y_5Si_3O_{12}N$
Pure Si	89.22	19.01	1.84	57.10	–	α Si_3N_4, β Si_3N_4, Si

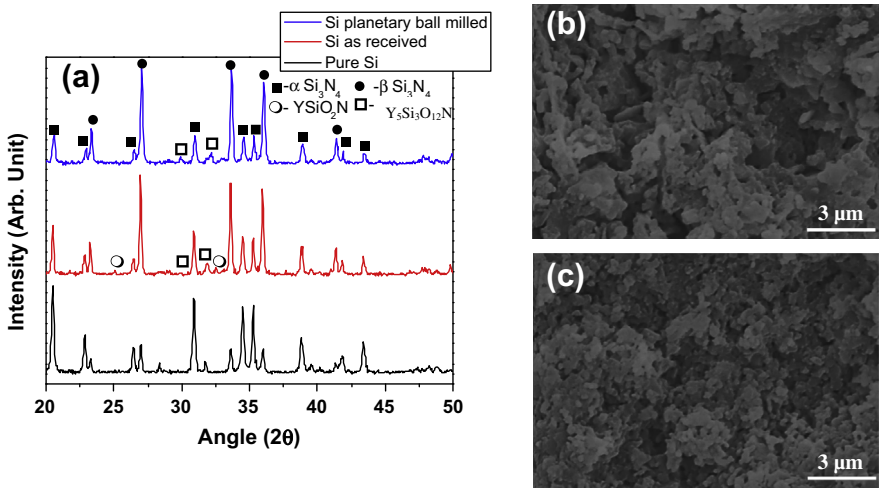

Fig. 2. (a) XRD patterns of the nitride bodies of Si_3N_4–3.5% Y_2O_3–1.5% MgO reaction bonded Si_3N_4 (RBSN) using Si as received and Si planetary ball milled powders. For comparison purpose the XRD pattern of pure Si without any sinter additive addition is also shown. (b) The SEM fracture surfaces of RBSN using Si as received and (c) Si planetary ball milled powders. The nitridation of all the samples were carried out at 1450 °C for 2.5 h.

large amount of β phase in RBSN sample of Si planetary ball milled powders can be attributed to the use of submicron size Si powders along with high amount of oxygen (as a result of planetary ball milling) in the powders. However, the nitridation of RBSN sample

Table 2
Linear shrinkage, weight loss, density, thermal diffusivity and thermal conductivity for Si_3N_4–3.5% Y_2O_3–1.5% MgO sintered reaction bonded Si_3N_4 (SRBSN) after gas pressure sintering at 1850, 1900 and 1950 °C for 3 h under 5 MPa N_2 gas pressure.

Sample	Linear shrinkage (%)			Weight loss (%)			Bulk density (g/cm^3)			Relative density (% ρ_{th})			Thermal diffusivity (cm^2/s)			Thermal conductivity (W/m K)		
	1850 °C	1900 °C	1950 °C	1850 °C	1900 °C	1950 °C	1850 °C	1900 °C	1950 °C	1850 °C	1900 °C	1950 °C	1850 °C	1900 °C	1950 °C	1850 °C	1900 °C	1950 °C
Si as received	13.78	13.56	14.26	1.67	1.75	2.54	3.11	3.12	3.19	96.25	96.67	98.68	29.24	38.44	41.14	62.39	82.56	89.61
Si planetary ball milled	11.03	11.17	10.29	2.16	2.69	2.41	3.21	3.21	3.18	99.47	99.49	98.55	21.69	25.43	23.98	47.46	55.77	51.94

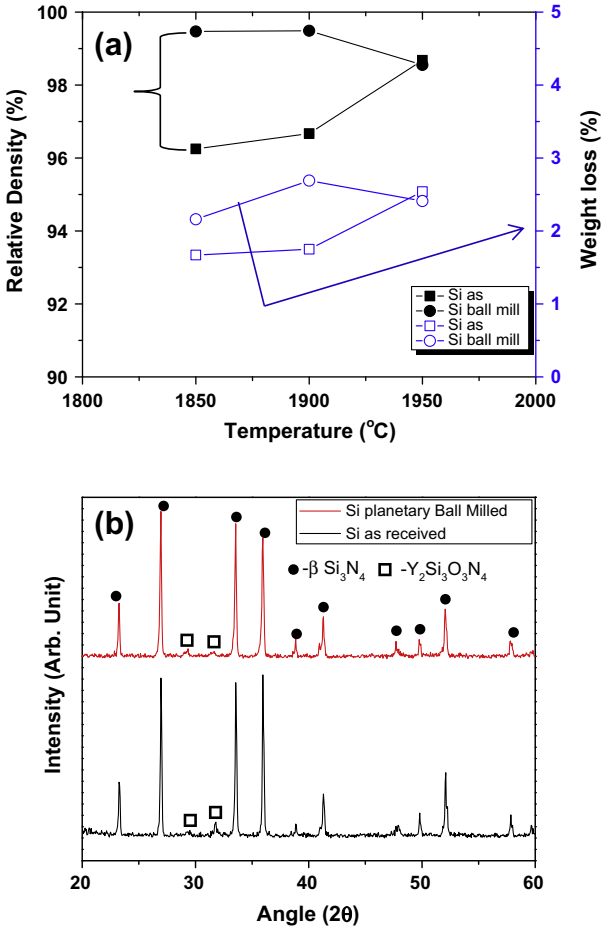

Fig. 3. (a) Relative density and weight loss as a function of sintering temperature of Si_3N_4–3.5% Y_2O_3–1.5% MgO sintered reaction bonded Si_3N_4 (SRBSN) using Si as received and Si planetary ball milled powders. Filled symbols represent the relative density and open symbols weight loss. (b) The cross sectional XRD patterns SRBSN samples after gas pressure sintering at 1950 °C for 3 h under 5 MPa N_2 gas pressure.

of Si planetary ball milled powders is relatively low, which imply that such Si powders characteristics show negative influence on the nitridation rate. The XRD of both the RBSN samples is shown in Fig. 2(a). Since there is no Si peak detectable in both the XRD patterns of RBSN samples with the sintering additive, it infers that the nitriding reaction is completed. Another interesting observation is the presence of a very small amount of secondary phases such as $YSiO_2N$ and $Y_5Si_3O_{12}N$ in the RBSN samples. The formation of these secondary phases can be attributed to the chemical reaction between rare-earth oxide, SiO_2 on the surface of Si particles and Si or newly formed Si_3N_4 during nitridation. However, no secondary phases containing Mg were detected by XRD. These XRD results are consistent with the literature for the RBSN processed with the similar sintering additive [5,29].

As a reference we also presented XRD pattern of RBSN sample without any sintering additive, which shows the presence of residual Si peak (see Fig. 2a and Table 1). It also can be noted here that RBSN sample without sintering additive has very strong α Si_3N_4 peaks, which is quite opposite to the RBSN samples mixed with the Y_2O_3–MgO sintering additive. Based on the results presented in Table 1, it can be said that sintering additive accelerates the nitridation reaction and enhances the densification by liquid phase formation during nitridation. Zhu et al. reported more than 95% nitridation, low amount of β Si_3N_4 phase (23.4%), relative density of 71.1% ρ_{th} for Si_3N_4–5 mol.% Y_2O_3–5 mol.% MgO after nitridation at 1400 °C for 8 h [29]. In another work, the RBSN with same

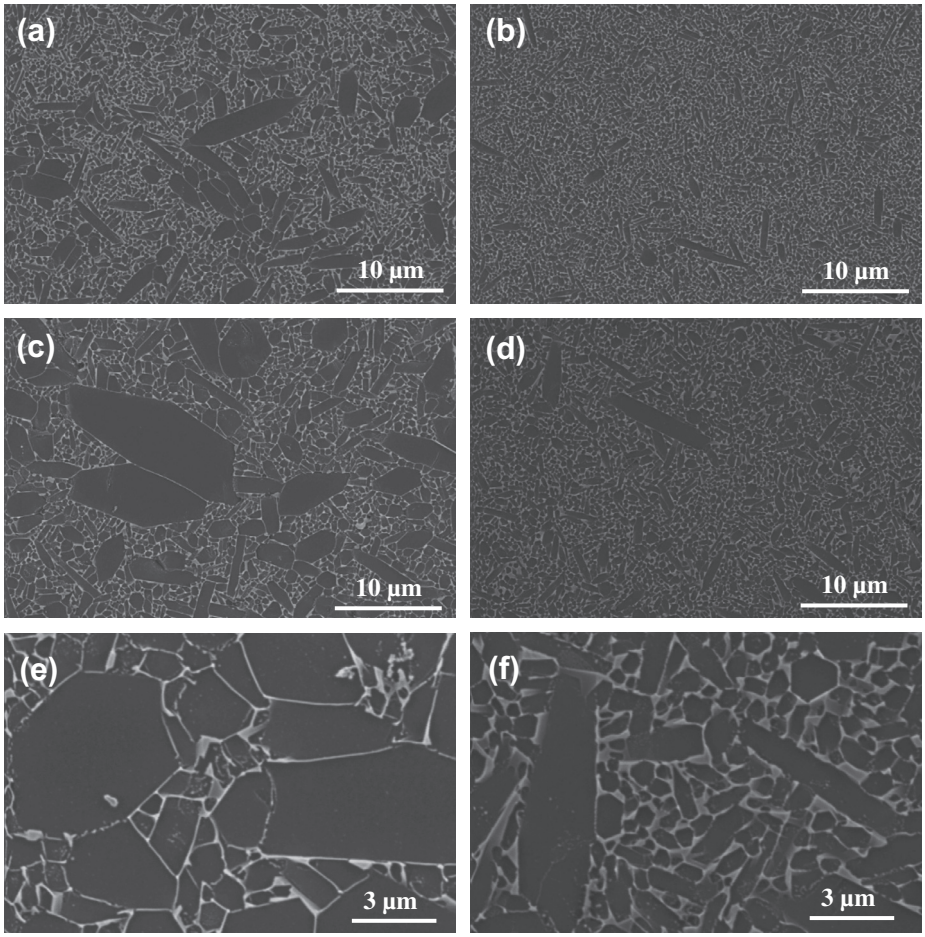

Fig. 4. The SEM microstructures of Si_3N_4–3.5% Y_2O_3–1.5% MgO SRBSN samples after sintering at 1850 °C for 3 h (a) using Si as received powders and (b) Si planetary ball milled powders, (c and e) SRBSN sample using Si as received powders after sintering at 1950 °C for 3 h and (d and f) SRBSN sample using Si planetary ball milled powders after sintering at 1950 °C for 3 h.

composition exhibited nitridation of 94%, β Si_3N_4 phase (12.6 wt.%) and relative density of 71% ρ_{th} after nitridation at 1350 °C for 8 h [25]. A comparison of these results with the present work reveals that nitridation processing conditions has significant effect on the nitridation characteristics of RBSN.

The SEM micrographs of fracture surfaces of the nitrided samples are shown in Fig. 2b and c. Both the RBSN samples with Si as received and Si planetary ball milled are characterized with porous microstructure. Most of the Si_3N_4 grains are equiaxed in agglomerated form for both the samples. In particular, RBSN sample with Si planetary ball milled shows a very fine uniform microstructure with equiaxed small grains (Fig. 2c). Intergranular fracture is the major mode of fracture in both the samples.

3.2. Densification and microstructural characterization

The characteristics of sintered specimens after the post-sintering (SRBSN) at different temperatures using gas pressure sintering are presented in Table 2. The relative density and weight loss of the samples as a function of sintering temperature are shown in Fig. 3a. It is observed that SRBSN samples using Si planetary ball milled powders are almost fully densified at all the sintering temperatures. In case of SRBSN samples using Si as received powders, the samples could be densified to ~97% ρ_{th} up to 1900 °C and it is increased to ~99% ρ_{th} with further increase of sintering temperature to 1950 °C. The densification of SRBSN samples clearly indicate that the very fine Si particle size and high amount of oxygen

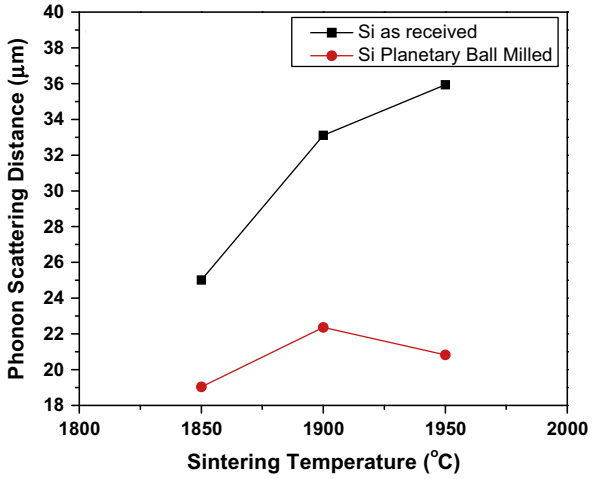

Fig. 5. The phonon mean free path of Si_3N_4–3.5% Y_2O_3–1.5% MgO SRBSN samples as a function of gas pressure sintering temperature.

in the Si powders after ball milling is aiding in densifying the RBSN samples relatively at lower sintering temperatures. On the other hand, the weight loss of both the samples increased with temperature up to 2.7%. However, the amount of weight loss for the samples with Si planetary ball milled is relatively high. Such high

amount of weight losses can be attributed to high oxygen content in the starting powders. These weight losses might have been due to the reaction between Si_3N_4 and SiO_2 (surface oxide layer on Si powders) during sintering:

$$Si_3N_4(s) + 3SiO_2(l) \rightarrow 6SiO(g) + 2N_2(g) \quad (3)$$

As a representative, XRD of SRBSN samples after sintering at 1950 °C for 3 h is shown in Fig. 3b. It has to be noted here that both samples exhibited similar XRD patterns at all the sintering temperatures. As α-Si_3N_4 was not detected in the SRBSN samples, it can be inferred that complete α–β phase transformation occurred under the sintering conditions. Crystalline β Si_3N_4 major phase and secondary $Y_2Si_3O_3N_4$ phases were observed in the samples after the gas pressure sintering. Fig. 4 shows SEM microstructures of SRBSN samples after sintering at 1850 and 1950 °C for 3 h. All the samples were basically made up of distinct bimodal microstructures with rod like grains distributed in fine matrix grains. The SRBSN sample of Si as received powders composed of very large elongated grains and fine matrix grains at both the sintering temperatures. However, more frequency of large elongated grains is noticeable at 1950 °C. On the contrary, the SRBSN sample with Si planetary ball milled powders microstructure is composed of very small elongated grains and very fine matrix grains at both the sintering temperatures (Fig. 4b and d). Nevertheless the grain size is relatively coarse for the sample sintered at 1950 °C when compared to the other sintering temperature.

3.3. Thermal conductivity

Table 2 also presents thermal diffusivities and thermal conductivities of SRBSN samples after sintering over a range of temperature from 1850 to 1950 °C for 3 h. It can be observed that the thermal diffusivity of SRBSN sample with Si as received powders increases significantly from 29.2–41.4 cm^2/s with increase of sintering temperature. A very small increase in thermal diffusivity (from 21.7 to 25.4 cm^2/s) with the sintering temperature is evidenced for the sample of Si planetary ball milled powders. Interestingly, the thermal conductivity significantly increased with temperature from 62.4 to 89.6 W/m K for the SRBSN sample with Si as received powders, whereas a slight increment in thermal conductivity up to 1900 °C and then it decreased with further increasing temperature for the SRBSN samples using Si planetary ball milled. The slight reduction in the sintered density and presence of large amount of grain boundary phase in the SRBSN samples using Si planetary ball milled might have caused such reduction in thermal transport properties for the samples after GPS at 1950 °C for 3 h. Zhu et al. made a comparative thermal conductivity study of SRBSN and sintered silicon nitride (SSN) using two different sintering additive compositions of Y_2O_3–MgO and Yb_2O_3–MgO [29]. They reported that a maximum thermal conductivity of 86 W/m K was achievable for SSN (irrespective of sinter additive type) and 93 W/m K was possible for SRBSN with 5 mol.% Yb_2O_3–5 mol.% MgO after gas pressure sintering at 1900 °C, for 6 h under a N_2 pressure of 1 MPa. In another work, Kusano and co-workers reported thermal conductivity of 89 W/m K for SRBSN (using low grade Si powder containing 1.6% impurity oxygen) with 5 mol.% Y_2O_3–5 mol.% MgO after gas pressure sintering at 1900 °C for 6 h [30]. They also reported that the thermal conductivity of the SRBSN can be improved to 100 W/m K by using a reagent grade high purity Si powder (containing 0.3% oxygen). In a different work, Zhu et al. reported that the thermal conductivity of SRBSN can be increased up to 133 W/m K by increasing gas pressure sintering time duration to 24 h at 1900 °C [31]. From this it can be said that proper selection of Si powders, sintering additive and sintering conditions is very important to improve thermal conductivity properties of SRBSN. In the present work, obtainment of thermal conductivity of ~90 W/m K for the SRBSN sample (using high purity Si as received powders) after gas pressure sintering at 1950 °C for shorter sintering time of 3 h is a promising result. Recently, Toshiba and Kyocera have been trying to use Si_3N_4 as a substrate material with active metal brazing (AMB) copper conductor for electronic applications [37,38]. The thermal conductivity of Si_3N_4 ceramics for such applications is reportedly varied from 58–90 W/m K [37,38,39]. Hence achieving thermal conductivity of 90 W/m K for Si_3N_4 ceramics via SRBSN after GPS for 3 h is beneficial for industrial applications.

In the present work, it is interesting to note that the SRBSN sample of Si as received powders exhibiting higher thermal diffusivity/conductivity at all sintering temperatures when compared to SRBSN samples using Si planetary ball milled powders despite its low densification. The existence of such differences in thermophysical properties of the samples can be attributed to its microstructure. Another possibility also can be due to the differences in the oxygen content of starting Si powders. Since the Si planetary ball milled powders were measured with high amount of oxygen, it might have resulted in excessive grain boundary phase.

According to Kitayama et al. the thermal conductivity of β Si_3N_4 at room temperature is controlled by the dissolved oxygen in the lattice of Si_3N_4, which causes phonon-defect scattering, thereby lowering the thermal conductivity [24]. The dissolution of oxygen in the β Si_3N_4 lattice results in the formation silicon vacancies, which scatter phonons and reduce phonon mean free path. It is well known that the phonon scattering plays a significant role in the thermal conductivity of ceramics. In order to understand the phonon scattering effects, the average phonon mean free path of Si_3N_4 samples is calculated from the measured thermal conductivity values. The resultant average phonon mean free path 'ι' is given by [40],

$$\iota = 3\frac{\lambda}{\upsilon C_p} \quad (4)$$

where λ is the thermal conductivity, υ the average sound velocity and C_p the specific heat capacity. A sound velocity of 11 km s^{-1} for Si_3N_4 is used to calculate phonon mean free path of SRBSN samples [41].

The average phonon mean free path in the SRBSN samples as a function of sintering temperature is shown in Fig. 5. The phonon mean free path increases (from 25 to 36 μm) with sintering temperature for the SRBSN sample with Si as received powders, whereas it varied narrowly from 19 to 22 μm for the SRBSN samples using Si planetary ball milled powders. Since the phonon mean free path is considerably larger than the grain size of SRBSN samples, depending on the sintering temperature it is expected that the phonons travel over less number of grains for SRBSN samples using Si as received powders when compared to SRBSN samples using Si planetary ball milled powders as the Si as received samples exhibits relatively coarse microstructure with bigger Si_3N_4 grains. The increase in thermal conductivity of samples with increase in sintering temperature can be mainly attributed to grain growth and large elongated β Si_3N_4 grains. The thermal conductivity of Si_3N_4 ceramics can be enhanced due to the promoted reduction of lattice oxygen content of β Si_3N_4 by enhanced grain growth via solution–reprecipitation process [28]. The increased fraction of large grains increases contiguity of β Si_3N_4–β Si_3N_4 , which leads to the improvement of thermal conductivity. Since the grain size of SRBSN samples using Si planetary ball milled powders possessed very fine grain microstructure, the phonon scattering by grain boundaries would be more and resulted in very low thermal conductivity when compared to the SRBSN sample of Si as received powders.

4. Conclusions

(a) The present investigation reveals that SRBSN sample of Si as received powders is advantageous as there is no need for Si particle size reduction (which adds up the processing cost and even increases oxygen content in the powders) and more importantly this sample exhibits relatively better thermal conductivity properties when compared to SRBSN using Si planetary ball powders. Although the use of fine powders are more effective in improving sinterability and properties of materials, the presence of high amounts of oxygen in the powders adversely affects thermal conductivity properties of SRBSN. Hence, future studies are needed to explore the possibility of reducing the Si particle size and controlling the oxygen content in the Si powders.

(b) The densification, thermal conductivity and phonon scattering distance of SRBSN samples are significantly affected by the Si particle size and the sintering temperature. The SRBSN sample using Si as received powders measured with maximum thermal conductivity of ~90 W/m K and phonon scattering distance of 36 μm after gas pressure sintering at 1950 °C for 3 h. The obtainment of such high thermal conductivity is encouraging to carry out more research for further increase in the thermal conductivity of SRBSN to a maximum extent by optimizing processing parameters.

References

[1] X. Zhu, Y. Zhou, K. Hirao, T. Ishigaki, Y. Sakka, Sci. Technol. Adv. Mater. 11 (065001) (2010) 1–11.
[2] T. Nishimura, X. Xu, K. Kimotoa, N. Hirosakia, H. Tanaka, Sci. Technol. Adv. Mater. 8 (2007) 635–643.
[3] F.L. Riley, J. Am. Ceram. Soc. 83 (2) (2000) 245–265.
[4] H. Klemm, J. Am. Ceram. Soc. 93 (6) (2010) 1501–1522.
[5] Y. Zhou, H. Hyuga, D. Kusano, Y. Yoshizawa, K. Hirao, Adv. Mater 23 (2011) 4563–4567.
[6] K. Hirao, Y. Zhou, H. Hyuga, T. Ohji, D. Kusano, J. Korean Ceram. Soc. 49 (4) (2012) 380–384.
[7] R. Kobayashi, Y. Moriya, M. Imamura, K. Oosawa, K. Oh-ishi, J. Ceram. Soc. Jpn. 119 (4) (2011) 291–294.
[8] H. Miyazaki, K. Hirao, Y. Yoshizawa, J. Eur. Ceram. Soc. 32 (2012) 3297–3301.
[9] H. Miyazaki, K. Hirao, Y. Yoshizawa, Mater. Sci. Eng. B 148 (2008) 257–260.
[10] R.G. Pigeon, A. Verma, A.E. Miller, J. Mater. Sci. 28 (1993) 1919–1936.
[11] A. Atkinson, A.J. Moulson, E.W. Roberts, J. Am. Ceram. Soc. 59 (3) (1976) 285–289.
[12] A.J. Moulson, J. Mater. Sci. 14 (5) (1979) 1017–1051.
[13] M.N. Rahaman, A.J. Moulson, J. Mater. Sci. 16 (8) (1981) 2319–2321.
[14] G. Ziegler, J. Heinrich, G. Wötting, J. Mater. Sci. 22 (1987) 3041–3086.
[15] J.R.G. Evans, A.J. Moulson, J. Mater. Sci. 18 (12) (1983) 3721–3728.
[16] J.A. Mangels, G.F. Tennenhouse, Am. Ceram. Soc. Bull. 59 (12) (1980) 1219–1222.
[17] B.W. Sheldon, J.S. Haggerty, Ceram. Eng. Sci. Proc. 10 (1989) 784–793.
[18] Z. Jovanovic, S. Kimura, O. Levenspiel, J. Am. Ceram. Soc. 77 (1) (1994) 186–192.
[19] B. Lei, O. Babushkin, R. Warren, J. Eur. Ceram. Soc. 17 (9) (1997) 1113–1118.
[20] M. Maalmi, A. Varma, W.C. Strieder, Chem. Eng. Sci. 53 (4) (1998) 679–689.
[21] M. Mueller, W. Bauer, R. Knitter, Ceram. Int. 35 (7) (2009) 2577–2585.
[22] B.T. Lee, J.H. Yoo, H.D. Kim, Mater. Sci. Eng. A 3333 (2002) 306–313.
[23] X. Zhu, Y. Zhou, K. Hirao, J. Mater. Sci. 39 (2004) 5789–5797.
[24] M. Kitayama, K. Hirao, K. Watari, M. Toriyama, S. Kanzaki, J. Am. Ceram. Soc. 84 (2) (2001) 353–358.
[25] X. Zhu, Y. Zhou, K. Hirao, J. Am. Ceram. Soc. 87 (7) (2004) 1398–1400.
[26] X. Zhu, Y. Sakka, Y. Zhou, K. Hirao, Acta Mater. 55 (2007) 5581–5591.
[27] N. Hirosaki, Y. Okamoto, F. Munakata, Y. Akimune, J. Eur. Ceram. Soc. 19 (12) (1999) 2183–2187.
[28] H. Yakota, S. Yamada, M. Ibukiyama, J. Eur. Ceram. Soc. 23 (2003) 1175–1182.
[29] X. Zhu, Y. Zhou, K. Hirao, J. Eur. Ceram. Soc. 26 (2006) 711–718.
[30] X. Zhu, Y. Zhou, K. Hirao, J. Am. Ceram. Soc. 89 (11) (2006) 3331–3339.
[31] X. Zhu, Y. Zhou, K. Hirao, Z. Lences, J. Am. Ceram. Soc. 90 (6) (2007) 1684–1692.
[32] D. Kusano, S. Adachi, G. Tanabe, H. Hyuga, Y. Zhou, K. Hirao, Int. J. Appl. Ceram. Technol. 9 (2) (2012) 229–238.
[33] D. Kusano, Y. Noda, H. Shibasaki, H. Hyuga, Y. Zhou, K. Hirao, Int. J. Appl. Ceram. Technol. 1–11 (2012), http://dx.doi.org/10.1111/j.1744-7402.2012.02767.x.
[34] H. Hayashi, K. Hirao, M. Toriyama, S. Kanzaki, J. Am. Ceram. Soc. 84 (12) (2001) 3060–3062.
[35] Y. Zhou, X. Zhu, K. Hirao, Z. Lences, Int. J. Appl. Ceram. Technol. 5 (2) (2008) 119–126.
[36] D.J. Delvin, K.E. Amin, Powder Diffr. 5 (3) (1990) 121–124.
[37] <http://www.toshiba.com/taec/Catalog/Line.do?familyid=20&lineid=7107>.
[38] <http://global.kyocera.com/prdct/semicon/power/amb/index.html>.
[39] B. Gaby, B. Dieter, S. Ina, P. Andreas, S. Jochen, Properties and Reliability of Silicon Nitride Substrates with AMB Copper Conductors, 44th International Symposium on Microelectronics, Long Beach, California USA, October 9–13, 000777–000784, 2011.
[40] K. Watari, H. Nakano, K. Sato, K. Urabe, K. Ishizaki, S. Cao, K. Mori, J. Am. Ceram. Soc. 86 (10) (2003) 1812–1814.
[41] J.C. Schon, A. Hannemann, G. Sethi, I.V. Pentin, M. Jansen, Process. Appl. Ceram. 5 (2) (2011) 49–61.